Fachtagung "Experimentelle Strömungsmechanik"
6.–8. September 2022, Ilmenau

Thermo-Elektro-Hydrodynamische Konvektion in einer dielektrischen Fluidschicht mit volumetrischer Erwärmung

Thermo-electrohydrodynamic convection in a dielectric fluid layer with volumetric heating

Matthias Strangfeld, Oguzhan Bölük, Peter S. B. Szabo, Martin Meier, Antoine Meyer, Yaraslau Sliavin, Vasyl Motuz, Christoph Egbers
Department of Aerodynamics and Fluid Mechanics, BTU Cottbus-Senftenberg, Cottbus, Germany

Thermische Konvektion, Elektrohydrodynamik, Dielektrophoretische Kraft, Plattenspalt
Thermal convection, Electrohydrodynamics, Dielectrophoretic force, Rectagular cavity

Abstract
Thermo-electrohydrodynamic (TEHD) convection is investigated in a dielectric fluid layer with internal volumetric heating and boundary heating. The experiment considered a stable stratified fluid layer with an a.c. voltage applied at the heated boundary to destabilise the flow to investigate the evolving TEHD convection by synthetic Schlieren. The voltage magnitude had a range of 2.5 to 17.5 kV with a frequency of 50Hz. The results suggest that TEHD convection onsets at below 7.5 kV that is in line with literature. When the voltage magnitude is increased, flow patterns emerge that are similar to those of the classical Rayleigh-Bénard convection cell. However, at higher voltages the volumetric heating increases and thus the flow become chaotic which could lead to large refraction angles that may not be captured by the particular measurement system.

Introduction
Thermal convection of a dielectric fluid layer in a horizontal plate cavity is investigated under the influence of an electrical force field. To provide a stable satisfied fluid layer the top and bottom plates of the cavity are maintained at two different temperatures T_1 and T_2, respectively. This provides a temperature difference of $\Delta T = T_1 - T_2 > 0$ within the fluid layer of thickness $d=10\ mm$. The effect of TEHD convection is provided by the so called dielectrophoretic effect that is induced in a dielectric fluid when an inhomogeneous electric field is applied in the presence of a temperature gradient (Pohl, 1978). Up till now scientises have been investigating this effect for several decades in different geometries such as in fluid layers (Roberts, 1969; Stiles, 1991; Stiles and Kagan, 1993), differentially heated cylinders (Chandra and Smylie, 1972; Futterer et al., 2016; Meier et al., 2018; Szabo et al., 2021; Yoshikawa et al., 2013) and spherical shells (Busse et al., 2003; Erdogdu et al., 2021; Futterer et al., 2012; Travnikov et al., 2003; Zaussinger et al., 2020). While the inhomogeneous electric field triggers the convection, the effect on the electric body force may differ between each geometry. Thus, the inhomogeneity in the electric field for cylindrical and spherical shells is majorly caused by the curvature whereas for the plate cavity an intrinsic temperature difference causes the inhomogeneous electric field (Mutabazi et al., 2016). In any case the force density is given by (Landau and Lifshitz, 1984) and written as

$$f_{EHD} = \rho_e E - \nabla\left[\frac{\rho}{2}\left(\frac{\partial \epsilon}{\partial \rho}\right)_T E^2\right] - \frac{E^2}{2}\nabla\epsilon \tag{1}$$

where ρ_e is the density of free charges, $\boldsymbol{E}$ the electric field, ϵ the electric permittivity and T the temperature. The first term on the right-hand side is the Columb force which can be neg-

GALA e.V., Karlsruhe, Germany, ISBN 978-3-9816764-8-8

lected if the thermal diffusion, charge relaxation, ion migration and viscose dissipation are much smaller than the oscillation period of the electric field (Turnbull, 1969). The second term is the electrostrictive force and has no effects on the flow if the fluid is incompressible and has no mobile boundaries (Zaussinger et al., 2018). The third term is the dielectrophoretic effects which is analogues to the Archimedean buoyancy. For small temperature differences, given by $\theta = T - T_0$, the electric permittivity, as well as the density, can be approximated by linear functions written as: $\epsilon = \epsilon_0 \epsilon_r (1 - e\,\theta)$ and $\rho = \rho_r (1 - \alpha\,\theta)$ where ϵ_0 is the electric permittivity in free space, ϵ_r the relative permittivity at reference temperature T_0 and α the thermal expansion coefficient. The two body forces may than be written for Archimedean buoyancy as $F_g = \rho_r \alpha\,\theta\, g$ and it is equivalent for the TEHD convection as $F_{DEP} = -\rho_r \alpha\,\theta\, g_e$ where g_e is expressed as an artificial electric gravity as suggested by (Roberts, 1969):

$$g_e = \frac{e}{\rho_r \alpha} \nabla \left(\frac{\epsilon_0 \epsilon_r E^2}{2} \right). \tag{2}$$

Hence, one can define the classical Rayleigh number as

$$Ra = \frac{\alpha\, \Delta T\, g\, d^3}{\nu\, \kappa} \tag{3}$$

and its electrical equivalent as

$$Ra_e = \frac{\alpha\, \Delta T\, g_o\, d^3}{\nu\, \kappa}. \tag{4}$$

Where ν is the kinematic viscosity, κ the thermal diffusivity of the fluid and g_0 the reference value of the artificial electric gravity by replacing the terrestrial gravity to formulate an expression for the TEHD convection, see Mutabazi et al. (2016).

For certain working fluids an a.c. voltage may cause volumetric heating by dielectric loss which arises e.g. from friction of the orientation and movement of the polarization state of molecules and can be defined by a temperature increase given by

$$\Delta T_{IH} = \frac{\epsilon_0 \epsilon_r \omega V_{RMS}^2 \tan\delta}{8\,\lambda}, \tag{5}$$

with the thermal conductivity λ. Equation (5) represents the equilibrium between the heating power – contributed by the dielectric loss – and the thermal diffusion (Yoshikawa et al., 2020). By replacing the temperature difference given by the boundaries of the cavity with the volumetric heating further Rayleigh numbers may be defined e.g. for terrestrial gravity a

$$Ra_{IH} = \frac{\alpha \epsilon \tan\delta\, g\, d^3\, \omega\, V_{rms}^2}{64\, \nu \kappa \lambda} \tag{6}$$

and for the electric equivalent as

$$Ra_{e,IH} = \frac{\varepsilon^3 e^2 \tan^2\delta\, \omega^2 V_{rms}^6}{256\, \rho\, \nu \kappa\, \lambda^2} \tag{7}$$

That follows the definition of (Yoshikawa et al., 2020). However, Yoshikawa et al. only investigated the internal heating case while here the case with boundary is investigated in addition. One can define appropriate relations to all Rayleigh numbers to obtain one characteristic number such as suggested in (Travnikov and Egbers 2021) as Rayleigh number ratios. With the above theoretical approaches experiments have been conducted by Turnbull (1969) in rectangular systems which we have further investigated.

The aim and objectives of this study is to investigate TEHD flow driven in the presence of terrestrial gravity and volumetric heating to investigate the potential TEHD flow for heat exchangers. In this particular study the onset of convection and the pattern formation is investigated which is captured by synthetic Schlieren technique. In the following section the experiment setup is discussed which is followed by an introduction of the synthetic Schlieren technique and the experiment procedure to record images. The recordings are than post treated to evaluate the results which are discussed in the following section. A conclusion is given at the end of the manuscript.

GALA e.V., Karlsruhe, Germany, ISBN 978-3-9816764-8-8

Experiment setup

To establish a horizontal fluid layer a rectangular cavity is designed to meet several requirements for investigating TEHD driven fluid flow with non-invasive optical measurement techniques. The housing of the rectangular cavity is built out of Polyoxymethylene (POM) and acrylic glass PMMA to ensure optical transparency for the light spectrum investigated and to guarantee electrical and thermal insulation. Furthermore, the field of view (FoV) over the width of the gap is ensured to provide optical access of the measurement system. The fluid gap is filled with a dielectric fluid. To investigate different gap properties the cavity can be geometrically modified in depth, length and width by varying the PMMA-inserts with different thicknesses between 3 and 10 mm. The bottom and top of the cavity are made out of borosilicate glass plates coated with ITO (Indium Tin Oxide) as transparent conductive oxide (TCO) to provide electrical conductive and thermal boundaries. One plate is connected to the electrical potential while the other is grounded. A high voltage (HV) generator with a peak voltage of up to 20 kV with a frequency range of up to 1000 Hz creates an electric field between the top and bottom plates. To maintain a temperature difference between the top and bottom plates cooling and heating loops are used which are filled with a silicone oil B5. The temperature stability within the loops are provided by a thermostat water bath and actively controlled by thermocouples which are located at each inlet and outlet of the cooling and heating channels. These control loops and a sufficient flowrate enable a homogeneous and an adequate temperature stability to provide a quasi-stable temperature difference between the two plates. To provide a uniform pressure onto the sealing a frame made out of

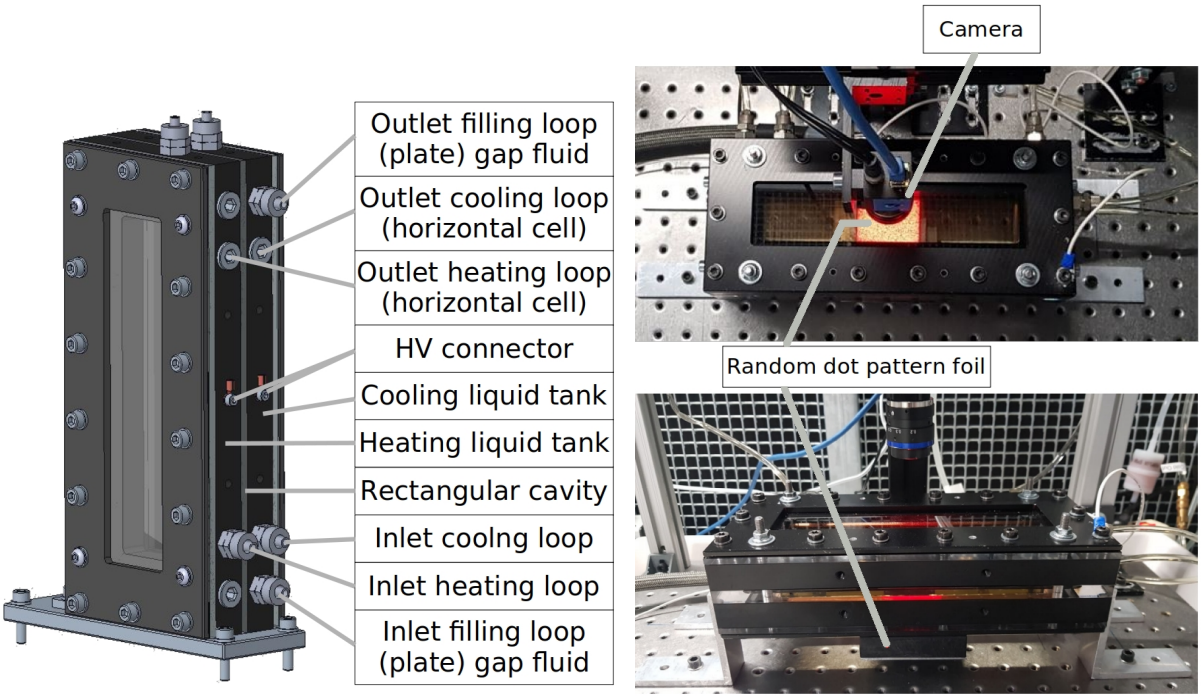

Figure 1: *Design of the plate cavity experimental cell (left) and the setup of the synthetic Schlieren technique for the horizontal plate cavity (right)*

aluminium is added to make sure that the whole experiment is tight. For the synthetic Schlieren technique a foil with a random dot pattern is used that is illuminated and recorded by a camera. The power of a planar LED-Array of 5.2 W was sufficient to illuminate the foil. On the opposite of the cavity a camera is mounted to observe an area of 50 by 40 mm. Thus, the dotted pattern, the dielectric fluid and the cooling and heating loops are therefore in the FoV of the synthetic Schlieren technique to investigate the effect of TEHD convection in a laboratory environment.

GALA e.V., Karlsruhe, Germany, ISBN 978-3-9816764-8-8

Synthetic Schlieren technique

The synthetic Schlieren technique – also known as Background orientated Schlieren (BOS) – utilises the changes in the refractive index that are caused by local variations the fluid's density. The relation of the refractive index to the density is given by the Lorentz-Lorenz equation. The light beams get refracted which leads to a refraction angle ε along the optical axis given by

$$\varepsilon_x = \frac{1}{n} \int \frac{\partial n}{\partial x} dz, \tag{8}$$

$$\varepsilon_y = \frac{1}{n} \int \frac{\partial n}{\partial y} dz \tag{9}$$

where n is the refractive index of the fluid (Settles and Hargather, 2017). The refracted light beams are captured by a camera mounted in the direction of the undisturbed FoV. With the distance between the camera and the fluid the absolute distance in refraction is given by Δx and Δy and can be calculated. To visualise the refraction the illuminated random dot pattern is used as described in the section above. With the light refraction the doted pattern is altered to the reference picture that is taken in an undisturbed case. The differences between both pictures can be calculated with a cross correlation algorithm. This is explained below in the section post processing. The result is a density gradient of the fluid which can be used to calculate the divergence field of the density to visualise uprising plumes that are indicative for convective flow. Hence, the synthetic Schlieren technique is able to produce quantitative measurement data with the support of the cross-correlation algorithm over a large FoV. In general, the technical requirement are easy to set up however limited the resolution to the traditional Schlieren technique that is simply related to the post processing algorithm that averages over a certain window size (Settles and Hargather, 2017).

Procedure

The measurement setup requires two main arrangements. The first deals with the convective flow which is control by the temperature difference and the a.c. voltage. The boundary temperature difference will be set up with the thermostat water bath while the applied difference is kept at 1 K for all experiment runs. The adjustment time of the system can be assumed to be in the range of the thermal diffusion given by $\tau = d^2/\kappa$. To ensure that there is a fully developed thermally stable stratified fluid layer the adjustment time in the experiment should be at least $1.5 \cdot \tau$. The high voltage system is triggered by a HV power supply unit. The system will therefore adjust to the changes. The recording of the measurement starts with the activation of the high voltage to capture the evolving flow fields. The second arrangement deals with the synthetic Schlieren setup. For this the LED array and the recording camera is activated and the focus of the camera is adjusted onto the random pattern foil to be able to take images that are in focus of the gap with an interval of one frame per second (fps). For the post processing a reference image of the random dot pattern foil is created for each parameter set. After stetting the system, the observation area (FoV) is investigated by capturing the recorded images for about 15 min for each measurement. The post processing will be done with a MatPIV algorithm by using MatLab that is explained in the following section.

Post processing

The post processing is realised with a MatLab-code which uses the MatPIV toolbox (Dalziel et al., 2000; Jongmanns, 2019). A cross correlation algorithm is used that finds it origin in post processing PIV images. To capture the refractive index changes a reference picture, see Figure 2 (a) is of need to compare the optical displacement based on the fluid's refractive index, see Figure 2 (b). The quantitative investigation is realised by creating converting the pixels (px) in the pictures to a real physical distance. In the next step the MatPIV algorithm is used to calculate the shifting between the flow and the reference picture by a cross correlation algorithm. Therefore, the picture is split into interrogation windows of the

GALA e.V., Karlsruhe, Germany, ISBN 978-3-9816764-8-8

size of 64 px x 64 px with an overlapping of 50 % afterwards the windows for the correlation gets iteratively smaller by half the size up to a size of 16 px by 16 px. A field of the refraction vectors can be calculated for each second of the measurements. To obtain the divergence field several filters are used to count for the errors. This is in particular the signal-to-noise ratio (snrfilt) which calculates the mean power of the used signal and divides it by the power of the background noise. Vectors smaller than a factor multiplied by the noise power will be changed to „NaN“ and thus no longer considered. A common factor is 1.3 which is used for our calculations (Keane and Adrian, 1992). The global histogram operator (globfilt) removes vectors with values significantly higher or smaller than the mean size of vectors. For realisation the global limits are determined by calculation of the mean value of all vectors plus or minus the standard deviation multiplied by a factor of 3.5. Similar to the global filter is the local filter that compares the vector size with those in adjacent direction. Therefore, a Kernel size – standard is 3x3 vectors – around the vector under investigation is created. If the value overrides the meridian plus or minus the threshold times the standard deviation of the Kernel the vector will be filtered out. The errors and out-filtered vectors are replaced with interpolation techniques due to the completeness of the vector field. Therefore, the “naninterp” filter function is used. The linear interpolation in the experiments sorts all outliers based on the number of spurious adjacent vectors and interpolates them from a low amount to the highest number of adjacent errors. So the places of NaN‘s can be filled. These filters are used to optimise the quality of the density gradient field which forms the base for the subsequent calculation of the divergence field.

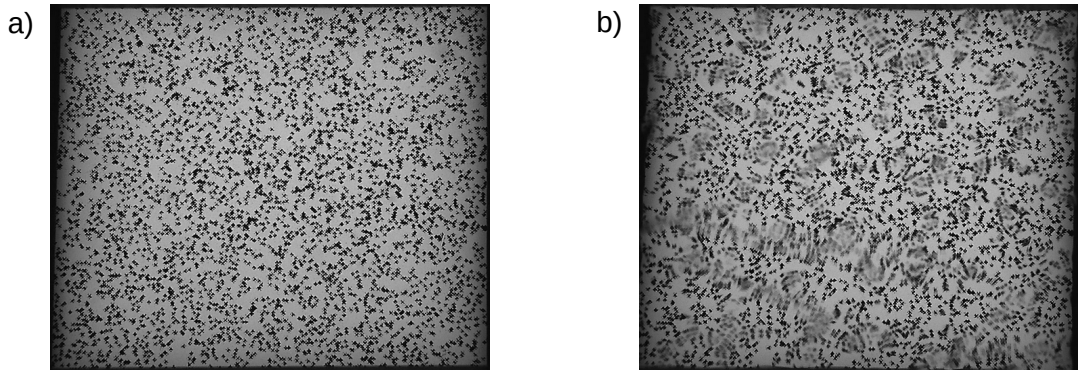

Figure 2: *Recorded raw pictures shown in (a) as a reference image with the undisturbed case and in (b) with displacement at V_{peak} =10 kV.*

Results

The results are obtained by the working fluid with 1-Nonanol with fluids properties shown in Table 1. Figure 3 shows the post processed divergence fields for different voltages applied. Due to the constant temperature difference the Rayleigh number for natural convection is kept constant at $Ra = 7254$ for all measurements. However, when applying the voltage a density change maybe visualised. For small voltages, see Figure 3 (a) no significant divergences are observed which is indicative that TEHD convection is unable to destabilise the stratified fluid layering. However, small disturbances are recorded in the density which may refer to the fluid flowing in the cooling and heating loops. When increasing the voltage the divergence is visible seen in Figure 3 (b) as not only the dielectrophoretic force but as well the volumetric heating increases and perturbates the fluid causing convective flow within the cavity that increase with voltage seen in Figure 3 (c) and (d). The effect is qualitatively observable by certain cell formation which are reminiscent of Marangoni-like patterns that can be described by arising Rayleigh-Bénard convections cells. Due to the transition in the voltages in the range of 2.5 kV to 7.5 kV a critical point can be assumed at which the flow becomes unstable and a dielectric driven convective flow under terrestrial gravity becomes visible. For voltages in the range of 7.5 kV < V_{peak} < 15 kV a quadrangular and pentagonal structures are visible in the divergence field, which is indicative of rising plumes of warmer fluid. *Therefore, a wavelength λ_p can be introduced which describes the distance of the central points of two neighboured structures. For 7.5 kV to 15 kV the wavelength is about* $\lambda_p \approx d/2$.

GALA e.V., Karlsruhe, Germany, ISBN 978-3-9816764-8-8

Table 1: *Fluid properties of 1-Nonanol for T=293K at a frequency of 50 Hz (Zaussinger et al., 2018)*

Property		Value	Dimension
Density	ρ	829.1	$kg \cdot m^{-3}$
Kinematic viscosity	ν	$1.4 \cdot 10^{-5}$	$m^2 \cdot s^{-1}$
Thermal diffusivity	κ	$7.94 \cdot 10^{-8}$	$m^2 \cdot s^{-1}$
Thermal conductivity	λ	0.16	$W \cdot K^{-1} \cdot m^{-1}$
Heat capacity	c_p	$2.470 \cdot 10^{3}$	$J \cdot kg^{-1} \cdot K^{-1}$
Coefficient of thermal expansion	α	$8.2344 \cdot 10^{-4}$	K^{-1}
Prandtl number	Pr	176	-
Thermal permittivity	e	$1.021 \cdot 10^{-2}$	K^{-1}
Energy dissipation factor	$tan\ \delta$	14.63	-
Refractive Index	n	1.43	-
Relative electric permittivity	ϵ_r	9.056	-

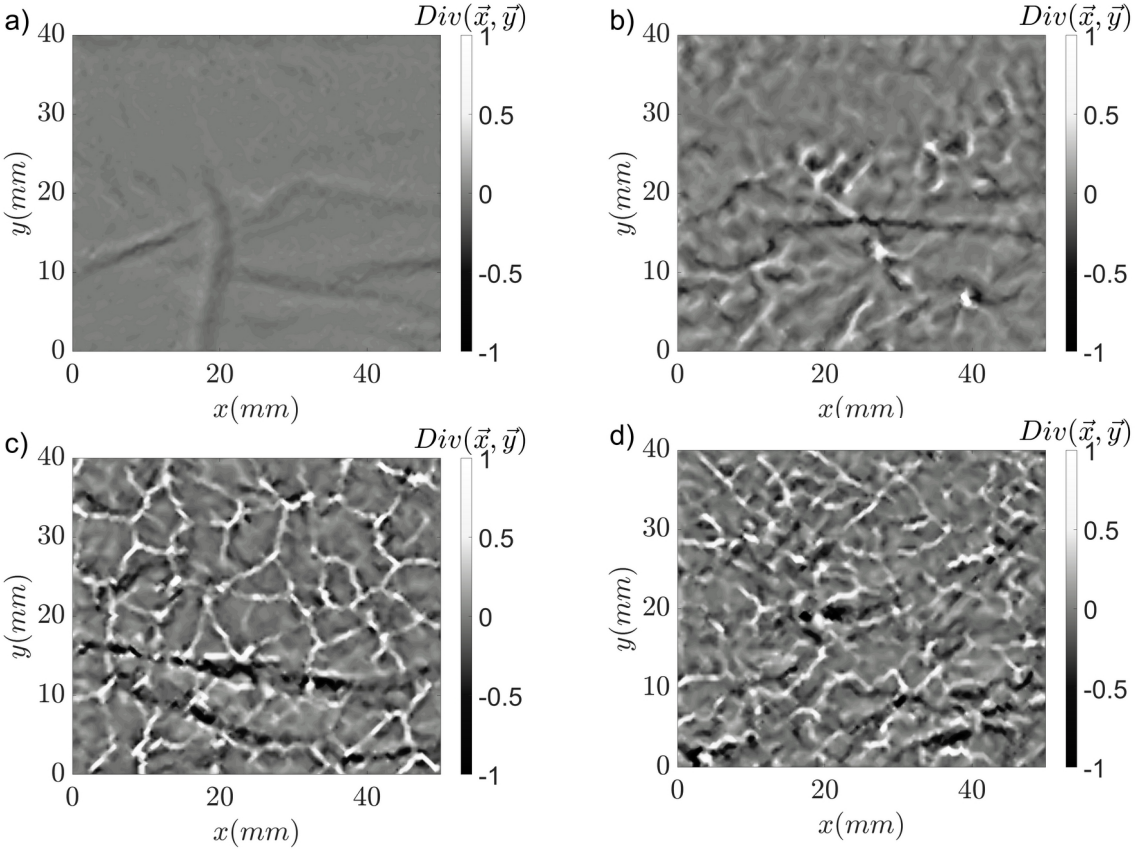

Figure 3: *Divergence field of the refractive index gradients for the range of applied voltages in (a) V_{peak} =2.5 kV, (b) V_{peak}=5 kV, (c) V_{peak}=10 k and V; (d) V_{peak}=17.5 kV.*

For larger voltages in the range of 15 kV to 17.5 kV the polygonal pattern appears to decrease and chaotic structures appear that are not clearly distinguishable as quadrangular and pentagonal structures. The reason could be related to a higher refraction angle that is present when the flow increases. However, the cross-correlation algorithm may run into difficulties that can be caused by the refraction of the dot pattern which is critical when individual dots are not any more clearly visible and thus are impossible to be tracked correctly. The influence of the internal heating is important to considered for this particular working fluid and of course cannot be neglected for higher voltages. This can be shown with the dimensionless number Υ for the comparison volumetric heat generation see (eq. 5) with the diffusion of thermal energy, given by (Yoshikawa et al., 2020). For $\Upsilon < 1$ the heat generation is smaller than the diffusion of thermal energy and therefore the influence of the volumetric heating is negligible. For $\Upsilon \geq 1$ the internal heating may influence the flow significantly for this particular working fluid. To provide an overview the particular number is shown in Table 2 for each

GALA e.V., Karlsruhe, Germany, ISBN 978-3-9816764-8-8

voltage. The occurrence of volumetric heating increases the convective flow and related to an internal temperature increase above the boundary temperature that can in addition cause convection within the system.

Table 2: *Characteristic numbers for the range of high voltages applied to the experimental system at a temperature difference of 1 K.*

V_{peak}	2500 V	5000 V	7500 V	10000 V	12500 V	15000 V	17500 V
Ra_e	28	113	255	453	708	1019	1387
T_{IH}	0.9	3.5	7.9	14.15	22.1	31.9	43.35
Ra_{IH}	802	3207	7217	12831	20048	28870	39295
$Ra_{e,IH}$	6	355	4040	22702	86601	$2.59 \cdot 10^5$	$6.52 \cdot 10^6$
Υ	7	29	65	115	180	259	353

Discussion

The experiment shows a clear development of convection within the thermally stable stratified fluid layering. This is due to the conducting TCO coating of the glass boundaries and the applied electric field inducing the dielectrophoretic force field together with volumetric dielectric heating of the working fluid 1-Nonanol fluid. This provides a destabilising effect and a development of convective flow within a stratified fluid by buoyancy. This effect leads to a temperature gradient and increase the heat transfers between the boundaries. The results show that the a.c. voltage can induce a force field that is strong enough to overcome the thermal stratification and is therefore enable to induce a convective flow. Thus, light refraction appears that is caused by the inhomogeneous density gradient cause by a temperature distribution. The recorded images provide a qualitative understanding of the flow and the resulting pattern that are comparable to Rayleigh-Bénard convection. For a quantitative statement the correlation between the refraction and the density gradient should be used in future experiments to calculate the temperatures out of the divergence field (Hayasaka et al., 2016). The qualitative results can be improved by increasing the frame rate of the camera and thus capture the movement of the polygonal structures in a better shape to make them traceable.

Conclusion

A high voltage is applied between the boundaries of an externally heated fluid layer to establish a dielectrophoretic volumetric force with volumetric internal heating. This force was able to destabilise the thermally stratified dielectric fluid layer and observed by synthetic Schlieren technique to visualise the evolving temperature fields by light refection. To investigate different cases an a.c. voltage of 50Hz was applied with its magnitude ranging form 1.5 kV to 17.5 kV with increment of 2.5 kV. Within the voltage range of 2.5 kV to 7.5 kV a critical point is found where the fluid layer destabilises due to the increasing dielectrophoretic force field. The recorded and post treated images show above the critical threshold polygonal structured pattern which are reminiscent to Rayleigh-Bénard convection cells. An interpretation of the pattern movement is not possible due to the low acquisition frequency. However, it is observed for voltage higher than 15 kV that polygonal structures decreases and the refraction becomes more chaotic. In addition, the introduced heating number Υ indicated that volumetric heating is not negligible for high voltage and shows some significant influences on the flow as was suggested by (Yoshikawa et al., 2020). The observed chaotic flow may occur due to the post processing progress and the large refractions of light that are not easy to be traced by the cross correlation algorithm. To determine the cause of the deceasing structures by higher voltages as well as the quantitative investigation of the temperature field by the divergence of the density gradient field needs to be further investigated.

Acknowledgements

The project “Thermoelektrische Konvektion unter Schwerelosigkeit (TEKUS)” is supported by the BMWi via the space administration of the Deutsches Zentrum für Luft und Raumfahrt (DLR) under Grant No. 50WM1944.

GALA e.V., Karlsruhe, Germany, ISBN 978-3-9816764-8-8

References

Busse, F.H., Zaks, M.A., Brausch, O., 2003. Centrifugally driven thermal convection at high Prandtl numbers. Physica D: Nonlinear Phenomena 184, 3–20.

Chandra, B., Smylie, D.E., 1972. A laboratory model of thermal convection under a central force field 3, 211–224.

Dalziel, S.B., Hughes, G.O., Sutherland, B.R., 2000. Whole-field density measurements by "synthetic schlieren." Experiments in Fluids 28, 322–335.

Erdogdu, A., Szabo, P., Carter, R., Gevrek, M., Haun, P., Zaussinger, F., Schulze, B., Meier, M., Egbers, C., 2021. Utilizing Wollaston shearing interferometry to investigate the refractive index gradient in a differentially heated annulus.

Futterer, B., Dahley, N., Egbers, C., 2016. Thermal electro-hydrodynamic heat transfer augmentation in vertical annuli by the use of dielectrophoretic forces through a.c. electric field 93, 144–154.

Futterer, B., Dahley, N., Koch, S., Scurtu, N., Egbers, C., 2012. From isoviscous convective experiment 'GeoFlow I' to temperature-dependent viscosity in 'GeoFlow II'—Fluid physics experiments on-board ISS for the capture of convection phenomena in Earth's outer core and mantle. Acta Astronautica 71, 11–19.

Hayasaka, K., Tagawa, Y., Liu, T., Kameda, M., 2016. Optical-flow-based background-oriented schlieren technique for measuring a laser-induced underwater shock wave. Experiments in Fluids 57, 179.

Jongmanns, M., 2019. Flow control of thermal convection using thermo electro hydrodynamic forces in a cylindrical annulus. Cuvillier Verlag.

Keane, R.D., Adrian, R.J., 1992. Theory of cross-correlation analysis of PIV images. Applied Scientific Research 49, 191–215.

Landau, L., Lifshitz, E., 1984. Chapter I–electrostatics of conductors. Electrodynamics of Continuous Media (Second Edition Revised and Enlarged) 1.

Meier, M., Jongmanns, M., Meyer, A., Seelig, T., Egbers, C., Mutabazi, I., 2018. Flow Pattern and Heat Transfer in a Cylindrical Annulus Under 1 g and Low-g Conditions: Experiments 30, 699–712.

Mutabazi, I., Yoshikawa, H.N., Fogaing, M.T., Travnikov, V., Crumeyrolle, O., Futterer, B., Egbers, C., 2016. Thermo-electro-hydrodynamic convection under microgravity: a review. Fluid Dynamics Research 48, 061413.

Pohl, H.A., 1978. Dielectrophoresis: The Behavior of Neutral Matter in Nonuniform Electric Fields.

Roberts, P.H., 1969. Electrohydrodynamic convection 22, 211–220.

Settles, G.S., Hargather, M.J., 2017. A review of recent developments in schlieren and shadowgraph techniques. Measurement Science and Technology 28, 042001.

Stiles, P.J., 1991. Electro-thermal convection in dielectric liquids. Chemical Physics Letters 179

Stiles, P.J., Kagan, M., 1993. Stability of cylindrical Couette flow of a radially polarised dielectric liquid in a radial temperature gradient 197, 583–592.

Szabo, P., Meier, M., Meyer, A., Barry, E.B., Motuz, V., Mutabazi, I., Egbers, C., 2021. PIV and shadowgraph measurements of thermo-electrohydrodynamic convection in a horizontal aligned differentially heated annulus at different gravity conditions. Experimental Thermal and Fluid Science 129, 110470.

Travnikov, V., Egbers, C., Hollerbach, R., 2003. The geoflow-experiment on ISS (Part II): Numerical simulation 32, 181–189.

Travnikov, V., Egbers, C., 2021. Numerical investigation of atmospherelike flows in a spherical geometry. Physical Review E, 104(6).

Turnbull, R.J., 1969. Electrohydrodynamic Rayleigh-Taylor Bulk Instability. Physics of Fluids 12, 1160.

Yoshikawa, H.N., Crumeyrolle, O., Mutabazi, I., 2013. Dielectrophoretic force-driven thermal convection in annular geometry 25, 024106.

Yoshikawa, H.N., Kang, C., Mutabazi, I., Zaussinger, F., Haun, P., Egbers, C., 2020. Thermoelectrohydrodynamic convection in parallel plate capacitors under dielectric heating conditions. Physical Review Fluids 5, 113503.

Zaussinger, F., Haun, P., Neben, M., Seelig, T., Travnikov, V., Egbers, C., Yoshikawa, H., Mutabazi, I., 2018. Dielectrically driven convection in spherical gap geometry 3, 093501.

Zaussinger, F., Haun, P., Szabo, P.S.B., Travnikov, V., Kawwas, M.A., Egbers, C., 2020. Rotating spherical gap convection in the GeoFlow International Space Station (ISS) experiment. Physical Review Fluids 5, 063502.

GALA e.V., Karlsruhe, Germany, ISBN 978-3-9816764-8-8